

Magnetization Plateaus in the Shastry-Sutherland Model for $\text{SrCu}_2(\text{BO}_3)_2$: Results of Fourth-Order Perturbation Expansion with a Low-Density Approximation

Yoshiyuki FUKUMOTO*

Department of Physics, Faculty of Science and Technology, Science University of Tokyo,
Noda, Chiba 278-8510

(Received)

Magnetization plateaus in the Shastry-Sutherland model for $\text{SrCu}_2(\text{BO}_3)_2$ are studied by the perturbation expansion method. The fourth-order effective Hamiltonian which describes the dynamics of triplet dimers (TD's) with $S_z^{\text{tot}} = 1$ in the singlet sea is derived and then partially diagonalized for the space that consists of the TD configurations with the lowest second-order energy. The fourth-order terms are treated within a low-density approximation. Our procedure makes clear how TD interactions are responsible for the formation of magnetization plateaus. Particularly, the 1/4-plateau is obtained by the fourth-neighbor TD repulsion in the fourth-order perturbation, and a diagonal stripe arrangement of TD's appears at this plateau.

KEYWORDS: $\text{SrCu}_2(\text{BO}_3)_2$, Shastry-Sutherland model, magnetization plateau, perturbation expansion, Heisenberg antiferromagnet, two dimensions

§1. Introduction

Two-dimensional frustrated Heisenberg antiferromagnets have been considerable interests for a long time because of unique magnetic properties which reflect unusual low-energy spectra due to a strong geometrical frustration. A typical example of such frustrated antiferromagnets is the spin-1/2 Kagomé antiferromagnet, where a disordered spin-liquid like ground state, a continuum of singlet excitations adjacent to the ground state, and gapped triplet excitations are obtained by numerical investigations.¹⁾

For the last two years, there has been a growing interest to a two-dimensional frustrated antiferromagnet which is called the Shastry-Sutherland model (SSM),²⁾ because Kageyama *et al.* and Miyahara and Ueda found that the SSM is realized in $\text{SrCu}_2(\text{BO}_3)_2$.^{3,4)} The Hamiltonian of the SSM under the uniform magnetic field H is defined by

$$\mathcal{H} = \sum_{\langle i,j \rangle} \mathbf{S}_i \cdot \mathbf{S}_j + \lambda \sum_{\langle\langle i,j \rangle\rangle} \mathbf{S}_i \cdot \mathbf{S}_j - MH, \quad (1)$$

where the first (second) term represents the intradimer (interdimer) coupling, and $M = \sum_i S_i^z$. (See Fig. 1.) Strength of the interdimer coupling in $\text{SrCu}_2(\text{BO}_3)_2$ is obtained to be $\lambda \sim 0.63$.^{5,6)} A distinctive feature of this model is that the orthogonal dimer structure shown in Fig. 1 leads to the exact dimer singlet ground state for $\lambda < \lambda_c$, and prohibits one-TD hopping up to the fifth order in λ .^{2,4)} As for the quantum phase transition at $\lambda = \lambda_c$, Koga and Kawakami obtained $\lambda_c = 0.68$ and

found that the exact dimer singlet ground state becomes to be unstable against the plaquette RVB state there.⁷⁾

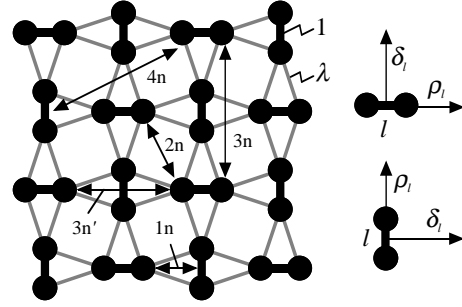


Fig. 1. Structure of a two-dimensional network formed by Cu^{2+} (closed circles) in $\text{SrCu}_2(\text{BO}_3)_2$. The vector ρ_l (δ_l) is the unit vector parallel (perpendicular) to the axis of a dimer at site l . The arrows indicate first-neighbor (1n), second-neighbor (2n), third-neighbor (3n, 3n') and fourth-neighbor (4n) dimer pairs. Note that there exist two types of third-neighbor dimer pairs. For brevity, we call that indicated by "3n" the third-neighbor pair.

Low-energy excitation spectra in the SSM have been investigated extensively because it is expected that the orthogonal dimer structure makes the spectra quite unique: the localized nature of one TD leads to a narrow band of scattering states of two TD's, while a TD pair with a short interdimer distance should have inherent dynamics in the multiplicity.^{8,9)} For instance, first-neighbor TD pair excitations can propagate through the third-order perturbation. As for experimental studies, in addition to the spin gap of 3.0 meV, the second spin gap

* E-mail: yfuku@ph.noda.sut.ac.jp

of 4.7 meV was observed by ESR and neutron inelastic scattering experiments.^{10,11} In particular, the neutron inelastic scattering experiment revealed that the second lowest triplet branch shows dispersive behavior although the lowest triplet branch is almost flat. In a Raman scattering experiment, a singlet excitation mode at 3.7 meV was observed.¹² These singlet and triplet bound states are considered to originate from first-neighbor TD pair excitations. On the other hand, first-neighbor TD pair excitations in the quintet sector lead to antibound states, and the lowest quintet branch consists of second-neighbor TD pair excitations. The lowest quintet branch shows rather weak dispersion, and the binding energy is much smaller than those of the singlet and triplet bound states.

The orthogonal dimer structure also gives rise to a unique feature of the magnetization process: $\text{SrCu}_2(\text{BO}_3)_2$ shows intermediate magnetization plateaus at $M = M_s/4$ and $M_s/8$, where M_s represents the saturated magnetization.³ To understand these plateaus, several groups derived the third-order effective Hamiltonian describing the dynamics of TD with $S_z^{\text{tot}} = 1$ in the singlet sea, and analyzed the resultant effective Hamiltonian.^{13,14,15,16} These investigations predicted the appearance of a 1/3-plateau, which was observed in a recent experiment.¹⁸ However, the origin of the 1/4- and 1/8-plateaus have not been clarified yet. Three scenarios to understand these two plateaus have been suggested. The first one is that these plateaus are produced by long-range TD repulsions due to higher-order perturbation. The second one is that some spin interactions omitted in the SSM play an essential role to realize these plateaus. For instance, it was shown that a magnetization plateau at $M = M_s/4$ is obtained in a generalized SSM.¹⁷ The third one is that the relevant cluster to understand these plateaus is not a spin dimer, but a spin plaquette, which is based on the fact that $\text{SrCu}_2(\text{BO}_3)_2$ locates near the dimer-to-plaquette phase boundary.⁷

In the present paper, we show that the fourth-order perturbation explains the 1/4-plateau invoking no additional spin interactions. We also describe in detail our previous brief report in Ref. 15 concerned with the third-order perturbation.

The present paper is organized as follows: in § 2, we derive the fourth-order effective Hamiltonian with a low-density approximation on the basis of the coupled dimer picture of the SSM. The fourth-order effective Hamiltonian is partially diagonalized for the subspace with the lowest second-order energy, and then the resultant Hamiltonian is analyzed by the numerical diagonalization method. In § 3, we give discussions about our calculation. It is particularly discussed how lower-order flip terms affect higher-order TD repulsions. In § 4, we summarize our results.

§2. Perturbation Expansion

2.1 Zeroth-Order Perturbation

We start with the dimer limit. Eigenstates of a dimer are the singlet state $|s\rangle$ and the triplet states $|t_1\rangle$, $|t_0\rangle$, $|t_{-1}\rangle$, where the suffix denotes the total S^z . The lowest energy states with magnetization $M(\geq 0)$ for the whole system consist of $|s\rangle$ and $|t_1\rangle$. We assume that the lowest energy states are in the degenerate space excluding $|t_0\rangle$ and $|t_{-1}\rangle$ when the interdimer coupling is taken into account.¹⁹ Then we calculate the fourth-order effective Hamiltonian

$$\mathcal{H}_{\text{eff}}^{4\text{PE}} = E_g + M(\Delta_{\text{sg}}^{4\text{PE}} - H) + \sum_{n=1}^4 \lambda^n V_n, \quad (2)$$

where

$$E_g = -\frac{3N_D}{4} \quad (3)$$

is the absolute ground state energy of the system with N_D dimers, and

$$\Delta_{\text{sg}}^{4\text{PE}} = 1 - \lambda^2 - \frac{\lambda^3}{2} - \frac{\lambda^4}{8} \quad (4)$$

is the fourth-order series of the spin gap. In eq. (2), V_n represents interaction among TD's in the n th-order perturbation. If the TD interaction leads to a kink in the minimum interaction energy per dimer, $\epsilon(m)$, as a function of density of TD's, $m(\equiv M/M_s)$, then a magnetization plateau is realized.

To write down the explicit form of V_n , it is convenient to introduce a pseudo-spin operator \mathbf{I}_l for each dimer site. The up and down spin states of \mathbf{I}_l correspond to the original dimer states as follows:

$$|\uparrow\rangle_l \leftrightarrow |t_1\rangle_l, \quad |\downarrow\rangle_l \leftrightarrow |s\rangle_l. \quad (5)$$

We also define the number operator of up spin and the spin-flip operator:

$$u_l \equiv \frac{1}{2} + I_l^z, \quad (6)$$

$$f_{l,l'} \equiv I_l^+ I_{l'}^- + I_l^- I_{l'}^+. \quad (7)$$

In terms of the original dimer states, u_l means the number operator of TD and $f_{l,l'}$ the hopping operator of TD.

2.2 First-Order Perturbation

The first-order interaction, V_1 , is calculated as follows:

$$V_1 = \frac{1}{2} \sum_{\langle l,l' \rangle \in 1\text{st}} u_l u_{l'}, \quad (8)$$

which is the nearest-neighbor Ising model on a square lattice. As is well known, TD's can be arranged on the square lattice avoiding first-neighbor TD pairs for $m \leq 1/2$, but can not for $m > 1/2$. The first-neighbor TD repulsion therefore leads to a kink in $\epsilon(m)$ at $m = 1/2$ as shown in Fig. 2, which means the appearance of 1/2-plateau. The Néel type arrangement of TD's is stabilized at the 1/2-plateau. The lower critical field of the 1/2-plateau is given by $\Delta_{\text{sg}}^{1\text{PE}} (= 1)$. The most important fact

is that all the configurations without first-neighbor TD pairs for $0 \leq m \leq 1/2$ degenerate at the critical field. So when another TD repulsion is taken into account, a new magnetization plateau is obtained even if the strength of the repulsion is small.

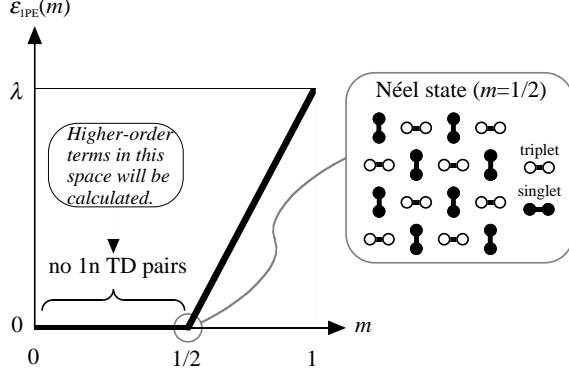


Fig. 2. First-order approximation of the minimum interaction energy $\epsilon_{1PE}(m)$ and TD configuration in the Néel state. The dimers with open (closed) circles are in the triplet (singlet) dimer state.

We are going to use the same argument to study if higher-order TD repulsions lead to additional plateaus. The situation becomes more and more complicated as the order of the perturbation becomes higher: in $\mathcal{H}_{\text{eff}}^{4PE}$, there exist many types of diagonal interactions and off-diagonal interactions. To overcome this difficulty, we utilize the fact of V_1 being a diagonal operator, which enables us to carry out partial diagonalization of $\mathcal{H}_{\text{eff}}^{4PE}$. To be precise, we direct our attention to the subspace without first-neighbor TD pairs for $m \leq 1/2$, in which the first-order energy is the lowest value. We write the new effective Hamiltonian as follows:

$$\bar{\mathcal{H}}_{\text{eff}}^{4PE} = E_g + M(\Delta_{\text{sg}}^{4PE} - H) + \sum_{n=2}^4 \lambda^n \bar{V}_n \quad \text{for } M \leq \frac{M_s}{2}, \quad (9)$$

where the constraint excluding first-neighbor TD pairs

$$\bar{u}_l \bar{u}_{l \pm \rho_l} = 0 \quad \text{for any } l \quad (10)$$

is imposed. The bar on operators means that the operators are defined in the constrained space.

2.3 Second-Order Perturbation

The second-order interaction, V_2 , is calculated as follows:

$$\begin{aligned} V_2 = & \frac{1}{2} \sum_{\langle l, l' \rangle \in 1n} u_l u_{l'} + \frac{1}{2} \sum_{\langle l, l' \rangle \in 3n} u_l u_{l'} - \frac{1}{2} \sum_l u_l u_{l+\rho_l} u_{l-\rho_l} \\ & + \frac{1}{4} (F_{1n \rightarrow 2n} + F_{2n \rightarrow 1n} + F_{1n \leftrightarrow 1n}). \end{aligned} \quad (11)$$

Here,

$$F_{1n \rightarrow 2n} = \sum_l (u_{l+\rho_l} - u_{l-\rho_l}) I_l^- (I_{l+\delta_l}^+ - I_{l-\delta_l}^+), \quad (12)$$

$$F_{2n \rightarrow 1n} = F_{1n \rightarrow 2n}^\dagger, \quad (13)$$

and

$$F_{1n \leftrightarrow 1n} = \sum_l u_l f_{l-\delta_l, l+\delta_l}, \quad (14)$$

are correlated hopping terms: $F_{1n \rightarrow 2n}$ ($F_{2n \rightarrow 1n}$) annihilates a first (second) neighbor TD pair and creates a second (first) neighbor TD pair, and $F_{1n \leftrightarrow 1n}$ annihilates a first-neighbor TD pair and creates another first-neighbor TD pair. As we will see below, $F_{1n \rightarrow 2n}$ and $F_{2n \rightarrow 1n}$ play a crucial role to produce an intermediate plateau at $m = 1/4$.

As mentioned previously, we calculate \bar{V}_2 in the subspace without first-neighbor TD pairs. Noting that the matrix elements of the three-body and correlated hopping terms are zero if initial and/or final states contain no first-neighbor TD pairs, we get

$$\bar{V}_2 = \frac{1}{2} \sum_{\langle l, l' \rangle \in 3n} \bar{u}_l \bar{u}_{l'}. \quad (15)$$

This equation shows that the third-neighbor TD repulsion dominates the low-energy physics in the second-order perturbation.

The third-neighbor TD repulsion in \bar{V}_2 increases the energy of the Néel state, which is the lowest energy state at $m = 1/2$, by $\lambda^2 N_D/4$. Thus the second-order perturbation leads to a new kink in $\epsilon(m)$. To determine the position of the kink, we calculate the second-order approximation of the minimum interaction energy, $\epsilon_{2PE}(m)$, for various finite size clusters up to $N_D = 36$. The shapes of clusters used in the present work are given in Fig. 3, where the periodic boundary condition is imposed. We show the result of $\epsilon_{2PE}(m)$ in Fig. 4. It is found that the kink appears at $m = 1/3$. The lowest-energy state at $m = 1/3$ is uniquely determined as the 1/3-stripe state which is defined in Fig. 4. This result is the same as the results obtained by Miyahara and Ueda¹³⁾ and Momoi and Totsuka.^{14,16)}

Equation (15) shows that no off-diagonal terms exist in the second-order interaction, which means that higher order terms may play an important role. Thus we can carry out partial diagonalization again. Then we study the subspace without first- and third-neighbor TD pairs for $m \leq 1/3$, which is the lowest energy states within the second-order approximation. We write this effective Hamiltonian in the following form:

$$\tilde{\mathcal{H}}_{\text{eff}}^{4PE} = E_g + M(\Delta_{\text{sg}}^{4PE} - H) + \sum_{n=3}^4 \lambda^n \tilde{V}_n \quad \text{for } M \leq \frac{M_s}{3}, \quad (16)$$

with the constraint

$$\tilde{u}_l \tilde{u}_{l \pm \rho_l} = \tilde{u}_{l+\rho_l} \tilde{u}_{l-\rho_l} = 0 \quad \text{for any } l. \quad (17)$$

The tilde on operators indicates the exclusion of first- and third-neighbor TD pairs.

As long as the interdimer coupling λ is small enough,

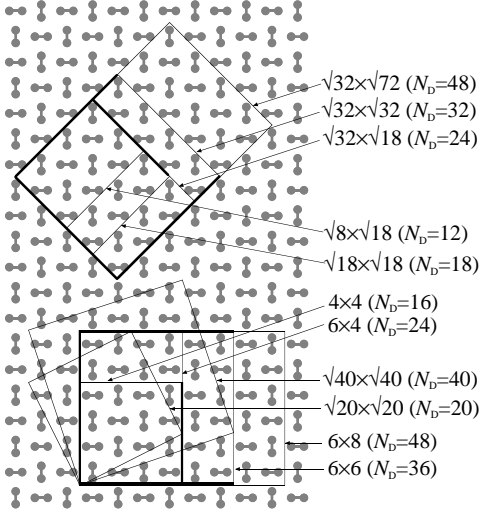


Fig. 3. Shapes of finite size clusters used in the numerical studies.

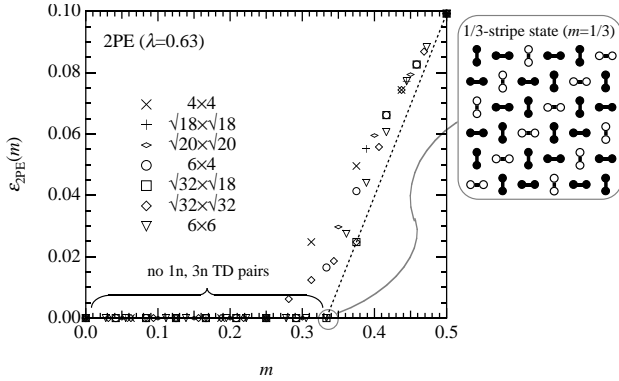


Fig. 4. Second-order results of minimum interaction energy, $\epsilon_{2PE}(m)$, at $\lambda = 0.63$, and TD configuration in the 1/3-stripe state.

the lowest energy states for $m \leq 1/3$ are in the subspace without first- and third-neighbor TD pairs due to TD repulsions up to the second-order perturbation. On the other hand, when λ is increased, the energy-gain due to TD hopping becomes to be more important than the TD repulsions. There should be an energy level crossing between these two regions. Our assumption for the restriction of the subspace is expected to be valid for wider range of λ as the density of TD's is lower, because the TD hopping in low-order perturbation is achieved by the correlated hopping. To check the validity of our perturbation theory for $\text{SrCu}_2(\text{BO}_3)_2$ with $\lambda \sim 0.63$, we use the exact diagonalization method and calculate the minimum interaction energy, $\epsilon_{ED}(m)$, on the 12-dimer cluster which matches the structure of the Néel and 1/3-stripe states. The result is shown in Fig. 5. We find no energy level crossing up to $\lambda \sim 0.63$, which means that the lowest energy states in $\text{SrCu}_2(\text{BO}_3)_2$ are adiabatically connected to the states retained in our perturbation the-

ory. This gives a support to the validity of our approach to $\text{SrCu}_2(\text{BO}_3)_2$.

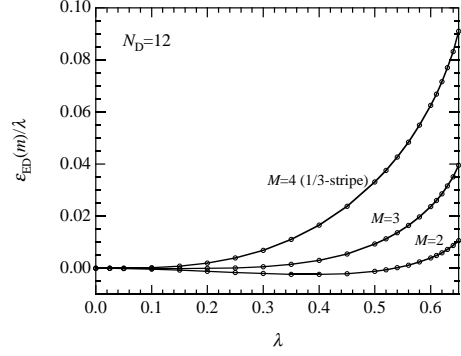


Fig. 5. Exact diagonalization results of the minimum interaction energy, $\epsilon_{ED}(m)$, for the 12-dimer cluster.

2.4 Third-Order Perturbation

We turn to the third-order interaction, V_3 . The calculation of this term is somewhat tedious, but can be achieved straightforwardly. The result is given by

$$V_3 = -\frac{1}{8} \sum_{\langle l, l' \rangle \in 1n} u_l u_{l'} + \frac{1}{4} \sum_{\langle l, l' \rangle \in 2n} u_l u_{l'} + \frac{3}{4} \sum_{\langle l, l' \rangle \in 3n} u_l u_{l'} + \frac{3}{8} F_{1n \rightarrow 2n} + \frac{1}{4} F_{2n \rightarrow 1n} + \frac{3}{8} F_{1n \leftrightarrow 1n} + (\text{three-body terms}). \quad (18)$$

We find in V_3 that second-neighbor TD repulsion appears for the first time in the third order. We also note that the coefficient of $F_{1n \rightarrow 2n}$ is different from that of $F_{2n \rightarrow 1n}$, i.e., V_3 is not an Hermite operator. All the off-diagonal terms in V_3 take the form of correlated hopping. The explicit expressions of the three-body terms are given in Ref. 16. The three-body terms, however, play no role in our treatment, because there are no matrix elements of the three-body terms in the subspace without first-neighbor TD pairs and we will use the two-body approximation in the fourth-order perturbation.

Using eqs. (8), (11) and (18), we obtain

$$\tilde{V}_3 = \frac{1}{8} \sum_l (\tilde{u}_{l+\rho_l} + \tilde{u}_{l+\rho_l})(\tilde{u}_{l+\delta_l} \tilde{u}_{l-\delta_l} + \tilde{f}_{l+\delta_l, l-\delta_l}). \quad (19)$$

Note that the second-neighbor repulsion exists in V_3 , but does not in \tilde{V}_3 . The processes which cancel the second-neighbor TD repulsion are shown in Fig. 6. We assume there exist two TD's at $l+\rho_l$ and $l+\delta_l$ in the initial state. Operating $(\lambda^2/4)F_{2n \rightarrow 1n}$ on the initial state, we get the intermediate states with a first-neighbor TD pair, whose energy is higher by $\Delta E = \lambda/2$ than the initial state. Operating $(\lambda^2/4)F_{1n \rightarrow 2n}$ on the intermediate states, we obtain the final state which is the same as the initial state. These second-order processes give a second-neighbor TD attraction $-(\lambda^3/4)\tilde{u}_{l+\rho_l}\tilde{u}_{l+\delta_l}$, which cancels the second-neighbor TD repulsion in the first-order process.

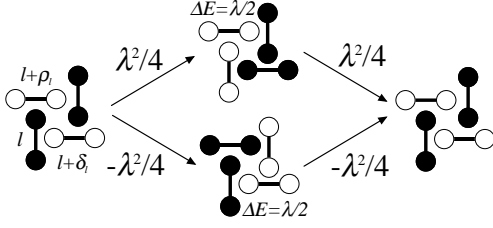


Fig. 6. Second-order processes which cancel the second-neighbor TD repulsion in V_3 . The number attached on each arrow represents the matrix element.

The third-order diagonal term in \tilde{V}_3 , which is a three-body repulsion, does not increase the energy of the $1/3$ -stripe state. Thus we obtain no plateau originating in the third-order effect. From this order, there exist correlated hopping terms. To study the effects of the correlated hopping terms on the magnetization curve, we diagonalize numerically \tilde{V}_3 on finite size clusters with $N_D = 24, 36$. The resultant magnetization curve at $\lambda = 0.63$ is shown in Fig. 7 together with the exact magnetization curve for the cluster with $N_D = 12$. The correlated hopping terms result in a finite width of the magnetic field region between $m = 0$ and $1/3$. However, this region is much narrower than that in the exact result. This result indicates that the energy-gain due to the third-order correlated hopping is rather small. So we expect that a magnetization plateau appears if there exists a TD repulsion responsible for a magnetization plateau in the next order.

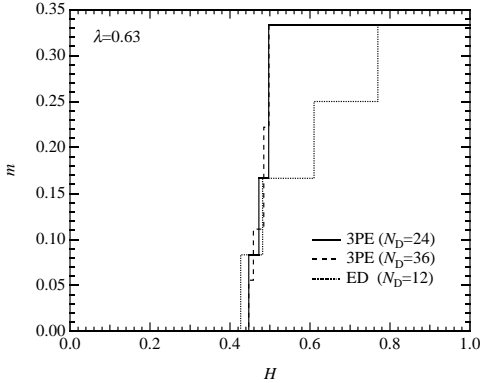


Fig. 7. Magnetization curve at $\lambda = 0.63$. The solid and long dashed lines are the results of the third-order perturbation (3PE), and the short dashed line is the result of the exact diagonalization (ED) of the SSM for the 12-dimer cluster.

2.5 Fourth-Order Perturbation

Up to now, all the perturbation processes have been taken into account in our calculation. In the fourth-order perturbation, such calculation is far from transparent. So we invoke the fact that we are now interested in low

density region of TD's, $m \leq 1/3$, and neglect three or more body terms in \tilde{V}_4 .

The fourth-order term V_4 takes the following form:

$$\begin{aligned}
 V_4 = & -\frac{9}{16} \sum_{\langle l, l' \rangle \in 1n} u_l u_{l'} + \frac{3}{8} \sum_{\langle l, l' \rangle \in 2n} u_l u_{l'} + \frac{1}{8} \sum_{\langle l, l' \rangle \in 3n} u_l u_{l'} \\
 & + \frac{1}{8} \sum_{\langle l, l' \rangle \in 4n} u_l u_{l'} - \frac{1}{32} F_{1n \rightarrow 2n} + \frac{9}{32} F_{2n \rightarrow 1n} + \frac{1}{8} F_{1n \leftrightarrow 1n} \\
 & + \frac{1}{16} \sum_l [(u_{l+2\rho_l+\delta_l} + u_{l+\delta_l} - u_{l+2\rho_l-\delta_l} - u_{l-\delta_l}) \\
 & \quad \times f_{l, l+\rho_l} - (\rho_l \rightarrow -\rho_l)] \\
 & + \frac{1}{32} \sum_l [(u_{l-\rho_l} + u_{l+2\rho_l+\delta_l} - u_{l+\rho_l} - u_{l+\delta_l}) \\
 & \quad \times f_{l, l+\rho_l+\delta_l} + (\delta_l \rightarrow -\delta_l)] \\
 & + \frac{1}{16} \sum_l [u_{l+\rho_l} (f_{l, l+2\rho_l+\delta_l} - f_{l, l+2\rho_l-\delta_l}) - (\rho_l \rightarrow -\rho_l)] \\
 & - \frac{1}{4} \sum_l (I_l^+ I_{l+\rho_l+\delta_l}^+ I_{l+\rho_l}^- I_{l+\delta_l}^- + \text{h.c.}) \\
 & + \frac{1}{32} \sum_l f_{l, l+\rho_l+\delta_l} f_{l+\rho_l, l+\delta_l} \\
 & + (\text{three or more body terms}). \tag{20}
 \end{aligned}$$

We find in V_4 that fourth-neighbor TD repulsion appears for the first time in the fourth order. The matrix element of the second-neighbor TD repulsion is three times as strong as that of the fourth-neighbor repulsion. As for the off-diagonal part, we find that TD pair hopping is possible from this order.

Calculation of matrix elements in the two-body approximation of \tilde{V}_4 is easily carried out by introducing the two-TD basis set in the momentum space, because it is reduced to partial diagonalization of a finite size matrix due to lack of the one-TD hopping. The result is given by

$$\begin{aligned}
 \tilde{V}_4 \simeq & \frac{1}{8} \sum_{\langle l, l' \rangle \in 4n} \tilde{u}_l \tilde{u}_{l'} \\
 & - \frac{1}{16} \sum_l [\tilde{f}_{l, l+\delta_l} (\tilde{u}_{l+\rho_l-\delta_l} - \tilde{u}_{l-\rho_l-\delta_l}) - (\delta_l \rightarrow -\delta_l)] \\
 & + \frac{3}{16} \sum_l \tilde{f}_{l, l+2\rho_l} (\tilde{u}_{l+\rho_l+\delta_l} + \tilde{u}_{l+\rho_l-\delta_l}) \\
 & - \frac{1}{16} \sum_l \tilde{f}_{l, l+2\delta_l} (\tilde{u}_{l+\rho_l+\delta_l} + \tilde{u}_{l-\rho_l+\delta_l}) \\
 & + \frac{1}{16} \sum_l [\tilde{f}_{l, l+2\rho_l+2\delta_l} \tilde{u}_{l+\rho_l+2\delta_l} + (\delta_l \rightarrow -\delta_l)] \\
 & - \frac{1}{4} \sum_l (\tilde{I}_l^+ \tilde{I}_{l+\rho_l+\delta_l}^+ \tilde{I}_{l+\rho_l}^- \tilde{I}_{l+\delta_l}^- + \text{h.c.}). \tag{21}
 \end{aligned}$$

Note that the second-neighbor TD repulsion exists in V_4 , but does not in \tilde{V}_4 . The processes which cancel

the second-neighbor TD repulsion are shown in Fig. 8. In Fig. 8(a), we use $(\lambda^2/4)F_{2n \rightarrow 1n}$ to obtain the intermediate states, and $(3\lambda^3/8)F_{1n \rightarrow 2n}$ to obtain the final state. In Fig. 8(b), we use $(\lambda^3/4)F_{2n \rightarrow 1n}$ to obtain the intermediate states, and $(\lambda^2/4)F_{1n \rightarrow 2n}$ to obtain the final state. These second-order processes (a) and (b) give second-neighbor TD attractions $-(3\lambda^4/8)\bar{u}_{l+\rho_l}\bar{u}_{l+\delta_l}$ and $-(\lambda^4/4)\bar{u}_{l+\rho_l}\bar{u}_{l+\delta_l}$, respectively. The process in Fig. 8(c) is a third-order one, where $(\lambda^2/4)F_{2n \rightarrow 1n}$ is used to obtain the intermediate states and $(\lambda^2/4)F_{1n \rightarrow 2n}$ is used to obtain the final state. This process gives a second-neighbor TD repulsion $(\lambda^4/4)\bar{u}_{l+\rho_l}\bar{u}_{l+\delta_l}$. Summing up the contributions of these three, we obtain a second-neighbor TD attraction of $-(3\lambda^4/8)\bar{u}_{l+\rho_l}\bar{u}_{l+\delta_l}$, which cancels the second-neighbor TD repulsion in the first-order process.

In \tilde{V}_4 , there exists the fourth-neighbor TD repulsion which increases the energy of the 1/3-stripe state by $\lambda^4 N_D/12$. The fourth-neighbor TD repulsion therefore leads to a kink in $\epsilon(m)$. To determine the position of the kink, we neglect TD hopping terms in $\tilde{\mathcal{H}}_{\text{eff}}^{4\text{PE}}$ and calculate the diagonal approximation of the interaction energy, $\epsilon_{4\text{PE}}^d(m)$, on various finite-size clusters up to $N_D = 48$. The result is shown in Fig. 9. It is found that there is the kink at $m = 1/4$. The lowest-energy state at $m = 1/4$ is uniquely determined as the 1/4-stripe state which is defined in Fig. 9.

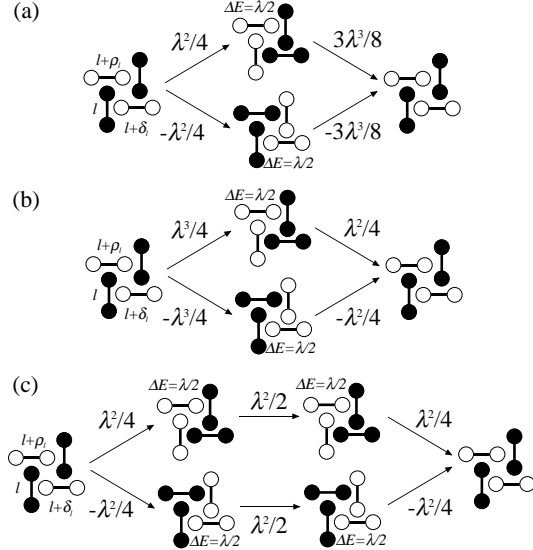


Fig. 8. Second- and third-order processes which cancel the second-neighbor TD repulsion in V_4 .

We calculate the magnetization curve of $\tilde{\mathcal{H}}_{\text{eff}}^{4\text{PE}}$ on the $\sqrt{32} \times \sqrt{18}$ cluster. The results are shown in Fig. 10 together with the second- and third-order results and the experimental result obtained by Onizuka *et al.*¹⁸⁾ In this figure, midpoints of each step due to hopping terms are connected by straight line to distinguish these from steps due to TD repulsions. Our theoretical result explains the

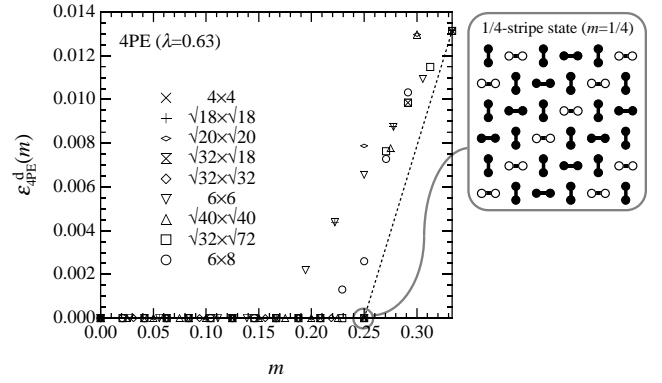


Fig. 9. Fourth-order results of minimum interaction energy $\epsilon_{4\text{PE}}^d(m)$, for the diagonal and low-density approximation of $\tilde{\mathcal{H}}_{\text{eff}}^{4\text{PE}}$, and TD configuration in the 1/4-stripe state, where we use $\lambda = 0.63$.

1/4-plateau observed experimentally. The width of the 1/4-plateau is also consistent with that of the experiment.

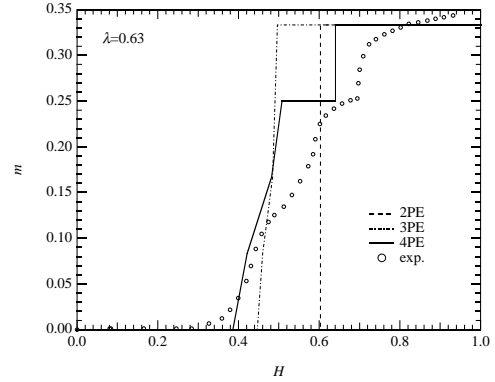


Fig. 10. Magnetization curve at $\lambda = 0.63$ calculated by using the perturbation expansion method up to the second order (2PE), the third order (3PE) and the fourth order (4PE). Calculations of the third- and fourth-order perturbation are carried out for the $\sqrt{32} \times \sqrt{18}$ cluster ($N_D = 24$). The circles represent experimental data obtained by Onizuka *et al.*¹⁸⁾ where we use the intradimer coupling 84 K and the g -value 2.05.

§3. Discussions

In our perturbation theory, we first calculate $\tilde{\mathcal{H}}_{\text{eff}}^{4\text{PE}}$, and then calculate $\tilde{\mathcal{H}}_{\text{eff}}^{4\text{PE}}$ for $m \leq 1/3$ in the subspace without first- and third-neighbor TD pairs. We here comment on the TD repulsions in these two Hamiltonians. In Fig. 11(a), we show the two-body repulsions in $\tilde{\mathcal{H}}_{\text{eff}}^{4\text{PE}}$. There exist first-, third-, second- and fourth-neighbor TD repulsions in $\tilde{\mathcal{H}}_{\text{eff}}^{4\text{PE}}$, which appear in the first-, second-, third- and fourth-order perturbation for the first time, respectively. At $\lambda = 0.63$, the matrix elements of these repulsions are given by 0.39, 0.41, 0.12 and 0.02 for first-, third-, second- and fourth-neighbor

TD pairs. In Fig. 11(b), we show all the repulsions in the low-density approximation of $\tilde{\mathcal{H}}_{\text{eff}}^{4\text{PE}}$. Here the first- and third-neighbor repulsions are treated as the constraint, which means that the matrix elements of these repulsions are approximated as the infinity. The other repulsions are the fourth-neighbor repulsion and the three-body repulsion.

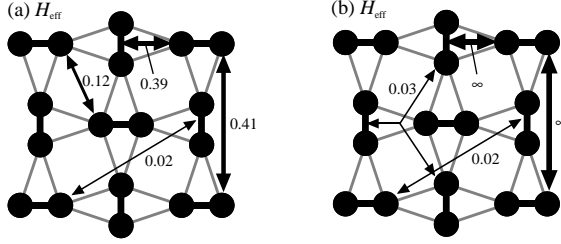


Fig. 11. Repulsions among TD's in (a) $\mathcal{H}_{\text{eff}}^{4\text{PE}}$ and (b) $\tilde{\mathcal{H}}_{\text{eff}}^{4\text{PE}}$. The number attached on each arrows represents the matrix element at $\lambda = 0.63$.

The vanishing of the second-neighbor TD repulsion in $\tilde{\mathcal{H}}_{\text{eff}}^{4\text{PE}}$ is essential to obtain the $1/4$ -plateau. To illustrate this, we consider the following Hamiltonian:

$$\begin{aligned} \tilde{\mathcal{H}}'_{\text{eff}} = & E_g + M(\Delta_{\text{sg}}^{4\text{PE}} - H) + \frac{\lambda^3(2 + 3\lambda)}{8} \sum_{\langle l, l' \rangle \in 2n} \tilde{u}_l \tilde{u}_{l'} \\ & + \frac{\lambda^4}{8} \sum_{\langle l, l' \rangle \in 4n} \tilde{u}_l \tilde{u}_{l'}, \end{aligned} \quad (22)$$

which is obtained by omitting the three-body repulsions and the second-neighbor TD attractions which originate from second- or third-order processes, and all flip terms from the low density approximation of $\mathcal{H}_{\text{eff}}^{4\text{PE}}$. Note that the second-neighbor TD repulsion is much stronger than the fourth-neighbor TD repulsion. We carry out the finite-size study of $\tilde{\mathcal{H}}'_{\text{eff}}$ using the clusters up to $N_D = 48$. In Fig. 12, we show the interaction energy, magnetization curve, and dimer configurations at plateaus. We find that there exist two plateaus at $m = 2/9$ and $1/6$, which contradict to the experimental results. It is obvious that the second-neighbor TD repulsion prevents the $1/4$ -plateau with the diagonal stripe TD arrangement. Thus, the $1/4$ -plateau is never obtained if one fails to notice the cancellation of the second-neighbor repulsion.²⁰⁾

It should be mentioned that the existence of the second-neighbor repulsion in $\mathcal{H}_{\text{eff}}^{4\text{PE}}$ from the third order has been known, and the possibility of the $1/4$ -plateau with the diagonal stripe TD arrangement has been pointed out.¹³⁾ However, it has remained as an open problem how this $1/4$ -plateau is stabilized although the second-neighbor repulsion exists. This question is resolved by the present results of the cancellation of the second-neighbor repulsion due to the correlated hopping terms of $F_{1n \rightarrow 2n}$ and $F_{2n \rightarrow 1n}$, and the existence of the fourth-neighbor repulsion in the fourth-order perturbation.

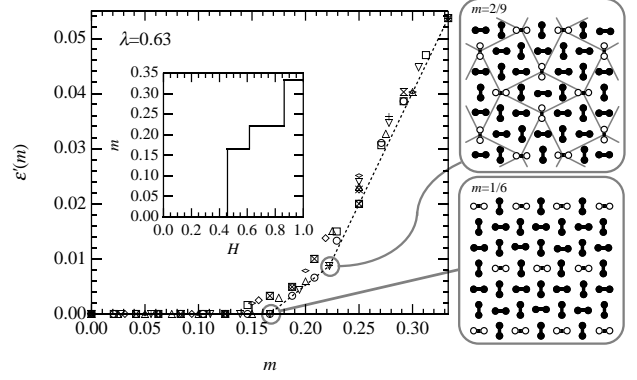


Fig. 12. Interaction energy, $\epsilon'(m)$, and the lowest energy configurations at $m = 2/9$ and $1/6$ for $\tilde{\mathcal{H}}'_{\text{eff}}$, where we use $\lambda = 0.63$. The correspondence of the symbols to the clusters is the same as that in Fig. 9. The inset shows the magnetization curve. In the configuration at $m = 2/9$, the interaction energy originates from the fourth-neighbor repulsion indicated by gray lines.

§4. Summary

We have been studied magnetization plateaus in the Shastry-Sutherland model. We have derived the fourth-order effective Hamiltonian, $\mathcal{H}_{\text{eff}}^{4\text{PE}}$, and then we have carried out partial diagonalization to get $\tilde{\mathcal{H}}_{\text{eff}}^{4\text{PE}}$ for the subspace without first- and third-neighbor triplet dimer pairs, in which second-order energy takes the lowest value. We have checked the validity of our approach to $\text{SrCu}_2(\text{BO}_3)_2$ by using the exact diagonalization method for the 12-dimer cluster. It has been shown that in the subspace excluding first-neighbor TD pairs the correlated hopping terms, $F_{1n \rightarrow 2n}$ and $F_{2n \rightarrow 1n}$, lead to the cancellation of the second-neighbor repulsion in $\mathcal{H}_{\text{eff}}^{4\text{PE}}$. Then the fourth-neighbor repulsion is responsible for the $1/4$ -plateau observed experimentally. At the $1/4$ -plateau, the diagonal stripe arrangement of TD's is stabilized.

Acknowledgements

The author would like to thank Professor A. Oguchi for useful discussions and critical reading of the manuscript. We have used a part of the codes provided by H. Nishimori in TITPACK Ver. 2.

-
- [1] P. Sindzingre, G. Misguich, C. Lhuillier, B. Bernu, L. Pierre, Ch. Waldtmann, H. U.-. Everts: *Phys. Rev. Lett.* **84** (2000) 2953.
 - [2] S. Shastry and B. Sutherland: *Physica* **108B** (1981) 1069.
 - [3] H. Kageyama, K. Yoshimura, R. Stern, N. V. Mushnikov, K. Onizuka, M. Kato, K. Kosuge, C. P. Slichter, T. Goto and Y. Ueda: *Phys. Rev. Lett.* **82** (1999) 3168.
 - [4] S. Miyahara and K. Ueda: *Phys. Rev. Lett.* **82** (1999) 3701.
 - [5] Z. Weihong, C. J. Hamer and J. Oitmaa: *Phys. Rev. B* **60** (1999) 6608.
 - [6] S. Miyahara and K. Ueda: *cond-mat/0004260*.
 - [7] A. Koga and N. Kawakami: *Phys. Rev. Lett.* **84** (2000) 4461.

- [8] Y. Fukumoto: J. Phys. Soc. Jpn. **69** (2000) 2755.
- [9] C. Knetter, A. Bühler, E. Müller-Hartmann and G. S. Uhrig: Phys. Rev. Lett. **85** (2000) 3958.
- [10] H. Nojiri, H. Kageyama, K. Onizuka, Y. Ueda and M. Motokawa: J. Phys. Soc. Jpn. **68** (1999) 2906.
- [11] H. Kageyama, M. Nishi, N. Aso, K. Onizuka, T. Yoshihama, K. Nukui, K. Kodama, K. Kakurai and Y. Ueda: Phys. Rev. Lett. **84** (2000) 5876.
- [12] P. Lemmens, M. Grove, M. Fischer, G. Güntherodt, V. N. Kotov, H. Kageyama, K. Onizuka and Y. Ueda: Phys. Rev. Lett. **85** (2000) 2605.
- [13] S. Miyahara and K. Ueda: Phys. Rev. B **61** (2000) 3417.
- [14] T. Momoi and K. Totsuka, Phys. Rev. B **61** (2000) 3231.
- [15] Y. Fukumoto and A. Oguchi: J. Phys. Soc. Jpn. **69** (2000) 1286.
- [16] T. Momoi and K. Totsuka: cond-mat/0006020.
- [17] E. Müller-Hartmann, R. R. P. Singh, C. Knetter and G. S. Uhrig: Phys. Rev. Lett. **84** (2000) 1808.
- [18] K. Onizuka, H. Kageyama, Y. Narumi, Y. Ueda and T. Goto: J. Phys. Soc. Jpn. **69** (2000) 1016.
- [19] M. Tachiki and T. Yamada: J. Phys. Soc. Jpn. **28** (1970) 1413.
- [20] Y. Fukumoto and A. Oguchi: Proc. ICM 2000 (in press).